Study of time-resolved luminescence in GaAs doping superlattices

W. Rehm, P. Ruden, G. H. Döhler, and K. Ploog
Max-Planck-Institut für Festkörperforschung, Heisenbergstrasse 1, D-7000 Stuttgart 80, Federal Republic of Germany
(Received 22 April 1983; revised manuscript received 13 July 1983)

The time-resolved observation of luminescence in GaAs doping superlattices yields valuable information about the peculiar decay of the excited state in these systems. The luminescence originates from the recombination of photoexcited charge carriers across the tunable effective energy gap. The shift of the luminescence spectrum to lower energies and its associated decrease in intensity after the excitation has ended are due to the increase in superlattice potential associated with the diminishing number of photoexcited charge carriers. Two sets of samples grown by molecular-beam epitaxy with different design parameters were investigated. The relation between energetic position and intensity of the luminescence spectrum was compared with results of self-consistent subband structure calculations, yielding good overall agreement. From the experiments, radiative and total lifetimes were determined as a function of the excitation level. It was found that the lifetimes vary over several orders of magnitude with only moderate changes of carrier concentration, confirming earlier predictions.

I. INTRODUCTION

The study of the luminescence properties of semiconductor superlattices has established itself as a valuable tool to gain information about the electronic structure of these materials.[1,2] In particular, the tunability of the luminescence in GaAs doping superlattices (*n-i-p-i* crystals)[3,4] has been demonstrated by a number of experimental studies on samples grown by molecular-beam epitaxy (MBE). These investigations have confirmed that the luminescence in doping superlattices is dominated by electron-hole recombination across the tunable indirect gap in real space, as predicted by theory.[5] In addition, the observation of tunable two-dimensional subbands by inelastic light scattering experiments[3] and the agreement between calculated and observed subband separations have provided unambiguous evidence that the impurity space-charge potentials act as one-dimensional quantum wells for the electrons.

The two-dimensional subband structure of GaAs doping superlattices should also be evident in the luminescence spectrum and in the lifetimes of the photoexcited carriers. Various broadening mechanisms, however, may obscure the observation of these phenomena. This broadening, at least to some extent, is an inherent property of the system, for instance, due to spatial potential fluctuations resulting from the random distribution of the impurities. In addition, it may be enhanced by the special experimental situation such as broadening due to inhomogeneous excitation. Finally, small deviations from the ideal superlattice periodicity due to variations of doping concentration or layer thickness may also cause broadening.

Time-resolved luminescence experiments represent an elegant tool for a detailed study of the time dependence of the position and shape of the luminescence spectrum and of the luminescence intensity. They are suitable for a discrimination between the above-mentioned classes of broadening phenomena. Luminescence experiments also allow one to separate out the lifetimes of various luminescent and nonluminescent decay processes of the photoexcited carriers.

A brief report of our first time-resolved luminescence measurements of GaAs doping superlattices has recently been published.[6] The present paper covers the results of a detailed study of time-resolved luminescence spectra and of photoexcited carrier lifetimes (radiative and nonradiative) for two sets of MBE-grown samples in which the doping level and the layer thickness were varied. The experimental results are compared with our recent calculations for superlattices with the corresponding design parameters.

The observed shape of the luminescence spectra indicates that broadening is mainly due to the statistical potential fluctuations associated with the random impurity distribution in the doping layers. Although the width of the luminescence spectra varies in a nonmonotonical way during the decay of luminescence, as expected from the theory, an unambiguous correlation between filling of subbands and observed luminescence spectra has not yet been established. The same is true for the (rather structureless) relation between the population of electronic subbands and the radiative lifetimes. The experimentally observed strong dependence of the radiative lifetimes on the degree of excitation, however, agrees well within the errors in design parameter control with the calculated behavior.

II. THEORY

The periodic sequence of positive and negative space-charge layers which exists in *n-i-p-i* superlattices leads to a modulation of the conduction and valence bands as has been described in detail elsewhere.[5] Charge carriers produced by photoexcitation in GaAs doping superlattices

thermalize on a very short time scale (psec) into the energetically most favorable states of the conduction and valence bands.[7] Thus the electrons occupy the quasi-two-dimensional subbands in the n-type layers while the holes populate a narrow impurity band above the valence band which is formed by the acceptor distribution in the p-type layers.[8] This effective energy gap may be called an indirect gap in real space (Fig. 1).

The transition probability for electron-hole recombination is proportional to the square modulus of the momentum matrix element between an electronic subband state and an impurity band state. In the effective-mass approximation this matrix element (we neglect the light-hole valence band) is proportional to the product of the bulk interband dipole matrix element and the overlap integral between the envelope function of the conduction subband $\Phi_{c,\mu}(z)$ (μ is the subband index and z is the space coordinate perpendicular to the layers) and an appropriate acceptor impurity-band envelope function $\Phi_{ib}(z-d/2)$, where d is the superlattice constant. We have

$$w_{\mathrm{rad}}(\mu) \propto \left| \int dz\, \Phi_{c,\mu}(z)\Phi_{ib}(z-d/2) \right|^2 . \tag{1}$$

The self-consistent calculation of the electronic subband envelope functions as a function of the carrier concentration has been discussed in detail in Ref. 8. The shape of the subband wave function changes dramatically over the range of carrier concentration accessible by photoexcitation. In particular the tails of the $\Phi_{c,\mu}(z)$ extend further and further into the p-type layers with increasing charge carrier concentration or (conversely) increasing effective energy gap. The tails of the envelope functions $\Phi_{ib}(z)$ of the holes in the impurity band can also be expected to change with the self-consistent superlattice potential.

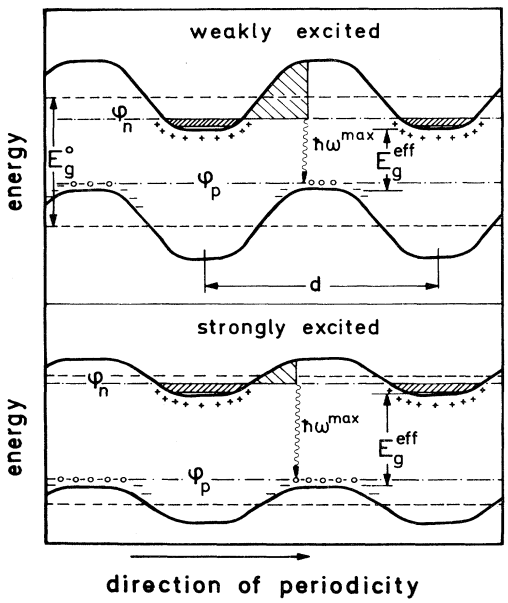

FIG. 1. Real-space energy-band profiles of a GaAs doping superlattice at two different excitation levels: E_g^0, GaAs band gap; E_g^{eff}, effective band gap depending on design parameters and exciting light intensity; and d, superlattice period.

The envelope functions $\Phi_{ib}(z)$ cannot be calculated in any straightforward way. To evaluate the transition probabilities as a function of the carrier concentration we have therefore replaced $\Phi_{ib}(z)$ by the uppermost heavy-hole valence-subband envelope function, ascribing to this, however, the energetic position of the single acceptor above the valence-band edge.

The wave vector parallel to the superlattice layers is not conserved in a transition involving the acceptor impurity band due to the random distribution of the impurities. In calculating the luminescence spectra we have therefore completely disregarded the $\vec{k}_{||}$-selection rule. Neglecting broadening effects this approach yields luminescence spectra, which have a steplike structure on the low-energy side, reflecting the superposition of the two-dimensional densities of states of the occupied conduction subbands weighted with the appropriate momentum matrix elements. On the high-energy side, given by the difference in quasi-Fermi levels of electrons and holes $\varphi_n - \varphi_p$, the luminescence intensity drops discontinuously from its maximum value to zero.

The steplike structure of the luminescence spectra can be expected to be very difficult to observe experimentally since the transition probabilities differ by almost an order of magnitude for neighboring subbands. The observed spectrum will therefore be dominated by transitions between the highest occupied conduction subband and the acceptor impurity band. Owing to the various broadening mechanisms listed in the Introduction the intensity in the low-energy tail of this specific transition may exceed the intensity of transitions from lower subbands.

At first sight, the subbands may be thought to be observable in the behavior of the total intensity $I(n^{(2)})$ or the lifetime $\tau_{\mathrm{rad}}(n^{(2)})$ with changing charge carrier concentration $n^{(2)}$. These quantities are given by

$$I(n^{(2)}) = \sum_{\mu} n_{\mu}^{(2)} w_{\mathrm{rad}}(\mu) \tag{2}$$

and

$$\tau_{\mathrm{rad}}(n^{(2)}) = n^{(2)}/I(n^{(2)}) , \tag{3}$$

where $n_{\mu}^{(2)}$ stands for the two-dimensional electron concentration in the μth subband. The slopes of I and τ_{rad} vs $n^{(2)}$ have discontinuities at those carrier concentrations at which a subband starts to become populated. Our numerical calculations, however, reveal that these discontinuities are too small to be observable in the systems studied. The luminescence peak position $E_p(n^{(2)})$ will be given by the center of gravity of the calculated spectra, assuming that the observed spectra are only broadened but not shifted in energy with respect to the calculated spectra.

With these approximations we have calculated the total luminescence intensity, peak position, and radiative recombination lifetime as a function of the carrier concentration by numerically integrating the one-dimensional effective Schrödinger equation[8] and using the eigenfunctions and eigenvalues in Eqs. (1)–(3). We find that due to the roughly exponential dependence of the tails of the wave functions entering the overlap integral in Eq. (1), the

luminescence intensity and the radiative-lifetime change over many orders of magnitude with only moderate changes in the charge carrier concentration. The rapid decrease in the luminescence intensity observed after switching off the excitation source is therefore not to be attributed to the decrease in the carrier concentration but rather to the decrease in the recombination probability.

III. EXPERIMENTAL

The photoluminescence experiments were performed on GaAs doping superlattices grown by MBE on semi-insulating (100)-oriented GaAs substrates. The constituent p-type and n-type layers were doped with Be and Si, respectively. Further details of the growth process were described in Ref. 9. Layer thickness and doping concentration were varied systematically in different superlattice configurations and are given in Table I for the samples used in the present study.

All photoluminescence experiments were carried out with the samples immersed in liquid He pumped to a temperature well below the λ point. The 647.1-nm line of a Kr^+ cw laser was used for excitation. The continuous emission of the laser was chopped by an acousto-optic modulator into pulses of typically 2 μs length and 40 μs repetition period. The pulse peak power was 250 mW and could be reduced by neutral-density filters without affecting the decay characteristics provided that the logarithmic time scale was adjusted correctly in order to take into account the changed starting conditions for the decay process.

The luminescence light was analyzed by a 0.75-m Spex single-grating monochromator. We used an S1 photomultiplier operated as a photon counter in order to extend the spectral range of the detection into the infrared region. We obtained the time information by gating the multiplier photon counts with pulses of adjustable delay with respect to the exciting light pulse.

IV. RESULTS AND DISCUSSION

Typical results of time-resolved luminescence experiments on GaAs doping superlattices are shown in Fig. 2. As expected, the normalized spectra shift to lower energies with increasing delay time, corresponding to the decrease of the effective band gap with the decreasing concentration of the excited carriers.[3–6] The spectra show a relatively broad asymmetric shape, very similar to steady-state spectra[4] with a steep slope on the high-energy side of the band. The time-resolved spectra change their shape

TABLE I. Design parameters.

Sample no.	$\tilde{d}=d_n=d_p$ (nm)	$n=n_D=n_A$ (10^{18} cm^{-3})
1	40	1
2	60	1
3	40	2
4	40	0.5
5	20	1

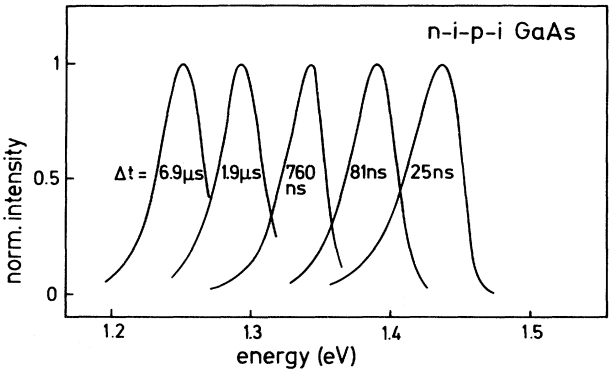

FIG. 2. Typical normalized luminescence spectra obtained from a GaAs doping superlattice during decay of photoexcited carriers (sample no. 1).

and become slightly more symmetric during the decay. The discussion of these properties will be given in a forthcoming paper.

A variation of the design parameters influences the recombination properties of doping superlattices strongly. Figure 3 shows the different luminescence peak shifts for various samples. In the set of samples with equal layer thickness but different doping concentration [Fig. 3(a)] the most heavily doped sample (no. 3) shows the fastest energy shift, whereas reduced doping results in a slower decrease of the effective band gap and, therefore, luminescence energy. A variation of layer thickness [Fig. 3(b)] results in a comparable set of curves. Here the sample with the thickest layers (no. 2) shows the fastest energetic decay. A modification of the peak excitation power does not affect the energetic shift provided the logarithmic time scale is adjusted correctly in order to take into account the changed starting conditions. That is the reason for the apparently different shape of the center curve (sample no. 1 in both parts).

Figure 4 shows the peak intensity versus time for both sets of samples. The figure indicates that those samples relaxing very fast to their ground state (largest doping concentration and thickest layers, samples nos. 3 and 2, respectively) also have the most pronounced intensity de-

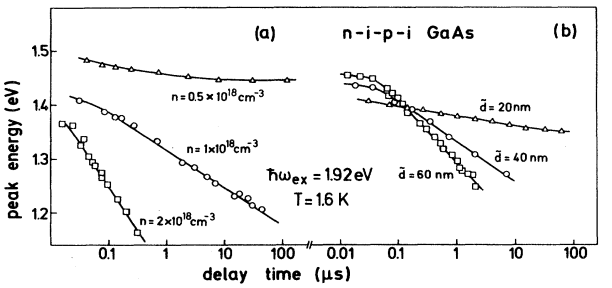

FIG. 3. Luminescence peak energy vs delay time for various samples of different doping concentration n [(a) left side, samples nos. 3, 1, and 4] and varied layer thickness $\tilde{d}$ [(b) right side, samples nos. 2, 1, and 5].

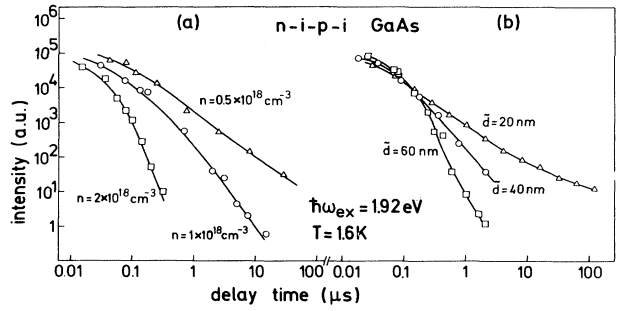

FIG. 4. Luminescence peak intensity vs delay time for various samples of different doping concentration n [(a) left side, samples nos. 3, 1, and 4] and varied layer thickness $\tilde{d}$ [(b) right side, samples nos. 2, 1, and 5].

cay. The curves are normalized to each other by their respective intensities at the end of the excitation, corresponding to a steady-state situation. Changes in the shape of the luminescence spectra are not taken into account but can be estimated to be a minor effect.

The basic results of Figs. 3 and 4 can be combined to a plot of intensity versus luminescence peak energy and compared with theory. The data points in Fig. 5 give the experimental peak intensity versus their respective peak energy. The solid curves are calculated as described in Sec. II using the design parameters listed in Table I. For a small shift in energy of about 0.2 eV the calculated and the experimentally determined intensities vary by several orders of magnitude and coincide for most samples over large parts. Deviations become slightly more pronounced for high excitation levels.

Samples nos. 4 and 5, i.e., the one with the thinnest layers and the one with the smallest doping concentration, show fairly large discrepancies between theory and experiment at low excitation levels. This can be attributed to possible deviations in their actual doping parameters with respect to those intended. At low excitation levels the relation I vs E_p becomes very sensitively dependent on the

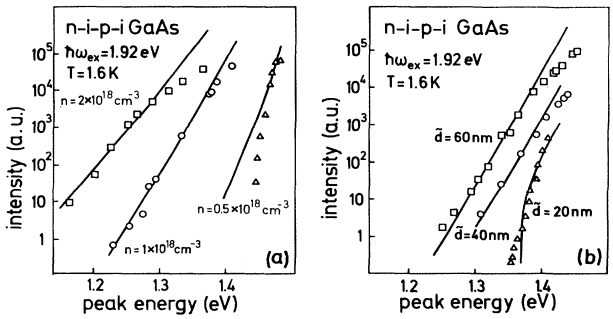

FIG. 5. Luminescence peak intensity vs respective peak luminescence energy for different doping concentration n [(a) left side, samples nos. 3, 1, and 4] and varied layer thickness $\tilde{d}$ [(b) right side, samples nos. 2, 1, and 5]. Solid lines show the results of calculations using the design parameters listed in Table I (see text).

design parameters. Even relatively small variations in the design parameters influence strongly the value of the effective band gap in the ground state. This gap corresponds to the photon energy at which the luminescence intensity drops to zero due to the lack of excited carriers. The other three samples investigated were, under experimental conditions, sufficiently far above the ground state.

We will now turn to a discussion of the lifetimes for photoexcited charge carriers in GaAs doping superlattices. The decay of the (two-dimensional) electron concentration is characterized by the total carrier lifetime $\tau_{\rm tot}$ according to

$$-\dot{n}^{(2)}=n^{(2)}\tau_{\rm tot}^{-1}(n^{(2)}) . \tag{4}$$

This total lifetime can be written as

$$\tau_{\rm tot}^{-1}(n^{(2)})=\tau_{\rm rad}^{-1}(n^{(2)})+\tau_{\rm oc}^{-1}(n^{(2)}) , \tag{5}$$

where $\tau_{\rm rad}^{-1}(n^{(2)})$ is the inverse lifetime for a radiative transition across the indirect gap in real space as described in Sec. II and $\tau_{\rm oc}^{-1}(n^{(2)})$ stands for a combined lifetime taking into account all other recombination channels. These include nonradiative transitions or radiative transitions other than the one mentioned above. Competing radiative transitions which are direct in real space have been observed previously in GaAs doping superlattices.[4] In the case of the samples discussed in the present work, however, the intensity of these recombination processes was found to be extremely small.

Luminescence experiments on GaAs doping superlattices allow for a determination of both the radiative lifetime $\tau_{\rm rad}(n^{(2)})$ and the total lifetime $\tau_{\rm tot}(n^{(2)})$. This most unusual feature of this type of superlattices is due to the one-to-one correspondence between charge carrier density and the energetic position of the luminescence spectra originating from a recombination across the effective energy gap. As noted previously[3] the nonequilibrium charge carrier concentration can be extracted from luminescence experiments by comparing the calculated peak energies (see Sec. II) with those measured.

In the present work we have applied this procedure to determine the charge carrier concentration as a function of time after the excitation has ended. The total lifetime is then given by

$$\tau_{\rm tot}(n^{(2)})=n^{(2)}(t)/\dot{n}^{(2)}(t) . \tag{6}$$

The radiative lifetime $\tau_{\rm rad}(n^{(2)})$ is determined from experiments by means of Eq. (3). Figure 6 shows the results for radiative and total lifetimes for the sets of samples with different doping concentration and with different layer thickness, respectively. Experimental points for the total lifetime cannot be given since the time derivative $\dot{n}^{(2)}(t)$ was determined from a smooth curve drawn through the experimental points of luminescence energy versus delay time.

The total lifetimes are plotted on an absolute scale. The radiative lifetimes on the other hand can only be given in arbitrary units since we did not determine absolute values of intensities. The results obtained from the thin layered sample are not included in Fig. 6(b) since luminescence was observed at energies smaller than the effective gap of

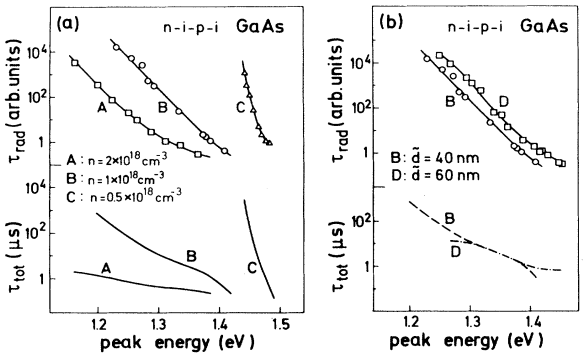

FIG. 6. Radiative (upper part) and total (lower part) lifetimes for various samples of different doping levels n [(a) left side, samples nos. 3, 1, and 4] and varied layer thickness $\bar{d}$ [(b) right side, samples nos. 1 and 2].

the nonexcited crystal (see Fig. 5), indicating a doping concentration larger than that intended. Again the expected trend is shown by every individual result. The lifetimes increase during the red shift of the luminescence over several orders of magnitude. An increase in the doping concentration without changing the layer thickness [Fig. 6(a)] obviously leads to a weaker dependence of the lifetimes on the peak energy. In the case of the radiative lifetime this can be understood as follows.

If the envelope functions involved in the overlap integral in Eq. (1) are replaced by the lowest harmonic-oscillator wave function for electrons and heavy holes, which should be a reasonable approximation at least for moderate excitation levels, the integral can be evaluated analytically, and one obtains for the radiative lifetime[10]

$$\tau_{\rm rad} \propto \exp\{(E_g^0 - E_p)/[(\hbar\omega_p^e + \hbar\omega_p^{hh})/4]\} , \qquad (7)$$

where the bulk-plasma frequencies ω_p^e for the electrons and ω_p^{hh} for the heavy holes are proportional to the square root of the doping concentration. Thus the slope of $\ln\tau_{\rm rad}$ vs E_p increases with decreasing doping concentration. Incidentally, it should be noted that the evaluation of Eq. (7) yields surprisingly good agreement with the rigorous calculations.

Considering now the total lifetime one should remark the fact that the difference in slope of $\ln\tau_{\rm rad}$ and $\ln\tau_{\rm tot}$ vs E_p is very pronounced for high doping and nearly disappears for low doping [Fig. 6(b)]. No information is available about nonradiative transitions in our material. It seems reasonable to assume that these processes have a large probability due to the high doping level and, therefore, high defect concentration.

There may, however, be another mechanism important in contributing to the total lifetime. Since under normal experimental conditions only a small spot of the sample is illuminated it can be expected that some charge carriers will also drift laterally into the nonilluminated region of the layers and thus be lost for recombination in the illuminated region. In the dark regions they too will eventually recombine. This, however, will be accompanied by a loss of energy corresponding to the effective gap in the nonexcited region which is smaller than the effective gap in the excited region of the superlattice. The loss in carrier concentration due to this lateral drift can also be taken as included in the inverse lifetime $\tau_{\rm oc}^{-1}(n^{(2)})$.

The probability for lateral drift of carriers into less-excited regions of the superlattice can be expected to be proportional to the electric fields parallel to the layers which increase with the difference between the values of the effective gap in the illuminated region and of the effective gap of the unexcited superlattice. The ground-state effective gap decreases with increasing doping concentration. The drift effect is therefore expected to become small for low peak energies close to the effective band gap in the ground state. Its relative importance with respect to the radiative recombination is, however, difficult to predict.

Changes in the layer thickness [Fig. 6(b)] lead to minor changes in the slope of the lifetimes versus peak energy only. In the case of the radiative lifetime this can also be understood on the basis of the approximate expression given in Eq. (7). The slope of $\ln\tau_{\rm rad}$ vs E_p there is independent of the layer thickness.

V. CONCLUSIONS

We have shown that time-resolved luminescence experiments can provide valuable information about the electronic structure of GaAs doping superlattices. Our experiments on several samples with different design parameters have confirmed the expected variation of the charge carrier lifetimes over many orders of magnitude associated with only moderate changes in the nonequilibrium carrier concentration. Self-consistently calculated luminescence intensities and radiative recombination lifetimes yield good agreement with the experimental results. The calculations shown use the intended design parameters of the superlattice only and involve no free parameters. Not only the radiative but also the total carrier lifetime was determined from the experiments.

Radiative and total carrier lifetimes can also be extracted from steady-state luminescence experiments. A detailed comparison of steady-state and time-resolved luminescence experiments on GaAs doping superlattices, particularly with respect to the various broadening mechanisms mentioned in the Introduction, will be a subject of future work.

ACKNOWLEDGMENTS

The authors are indebted to A. Fischer for expert help in sample preparation, to W. Heinz for technical assistance with the luminescence measurements, and to H. Jung and H. Künzel for stimulating discussions. Part of this work was sponsored by the Bundesministerium für Forschung und Technologie of the Federal Republic of Germany.

[1]C. Weisbuch, R. C. Miller, R. Dingle, A. C. Gossard, and W. Wiegmann, Solid State Commun. 37, 219 (1981).
[2]E. E. Mendez, G. Bastard, L. L. Chang, L. Esaki, H. Morkoc, and R. Fischer, Phys. Rev. B 26, 7101 (1982).
[3]G. H. Döhler, H. Künzel, D. Olego, K. Ploog, P. Ruden, H. J. Stolz, and G. Abstreiter, Phys. Rev. Lett. 47, 864 (1981).
[4]H. Jung, G. H. Döhler, H. Künzel, K. Ploog, P. Ruden, and H. J. Stolz, Solid State Commun. 43, 291 (1982).
[5]G. H. Döhler, Phys. Status Solidi B 52, 79 (1972); 52, 79 (1972).
[6]W. Rehm, H. Künzel, G. H. Döhler, K. Ploog, and P. Ruden, Physica 117-118B, 732 (1983).
[7]D. von der Linde and R. Lambrich, Phys. Rev. Lett. 42, 1090 (1979).
[8]P. Ruden and G. H. Döhler, Phys. Rev. B 27, 3538 (1983).
[9]K. Ploog, A. Fischer, and H. Künzel, J. Electrochem. Soc. 128, 400 (1981).
[10]G. H. Döhler, J. Vac. Sci. Technol. B 1, 278 (1983).